

# Fixing the Energy Scale in Scanning Tunneling Microscopy on Semiconductor Surfaces

Gerhard Münnich,<sup>1</sup> Andrea Donarini,<sup>2</sup> Martin Wenderoth,<sup>3</sup> and Jascha Repp<sup>1</sup>

<sup>1</sup>*Institute of Experimental and Applied Physics,  
University of Regensburg, 93053 Regensburg, Germany*

<sup>2</sup>*Institute of Theoretical Physics, University of Regensburg, 93053 Regensburg, Germany*

<sup>3</sup>*IV. Physikalisches Institut der Georg-August-Universität Göttingen,  
Friedrich-Hund-Platz 1, 37077 Göttingen, Germany*

(Dated: June 6, 2022)

## Abstract

In scanning tunneling experiments on semiconductor surfaces, the energy scale within the tunneling junction is usually unknown due to tip-induced band bending. Here, we experimentally recover the zero point of the energy scale by combining scanning tunneling microscopy with Kelvin probe force spectroscopy. With this technique, we revisit shallow acceptors buried in GaAs. Enhanced acceptor-related conductance is observed in negative, zero, and positive band-bending regimes. An Anderson-Hubbard model is used to rationalize our findings, capturing the crossover between the acceptor state being part of an impurity band for zero band bending, and the acceptor state being split off and localized for strong negative or positive band bending, respectively.

Since its invention, the scanning tunneling microscope (STM) has been widely used to study semiconductor surfaces. The qualitative interpretation of such studies can be obscured by the presence of tip-induced band bending  $\text{TIBB}(V)$ , i.e., by the bias-dependent shift of all electronic states beneath the microscope's tip [1–3]. If shifted across the Fermi level,  $\text{TIBB}(V)$  changes the average occupation of an electronic state, which, in turn, determines if this state contributes to the electronic transport within the junction [4–8]. However, since the contact potential difference (CPD) between tip and sample is, with few exceptions [9, 10], unknown in STM, within the relevant bias range, not even the sign of  $\text{TIBB}(V)$  is known. In this context, the conductance spectra of shallow acceptors buried in III–V semiconductor hosts remained a puzzle unsolved for almost two decades: depending on the sign of the band bending assumed or inferred from scanning tunneling spectroscopy (STS), conductance is explained either due to tunneling of electrons into empty acceptor states (positive TIBB) [11], or due to a modification of the tunneling barrier by the occupied acceptor (negative TIBB) [9], or by the empty acceptor state being in resonance with an impurity band (zero TIBB) [12]. Although the need for an exact value of the CPD has clearly been recognized [9, 12], bare STM-based methods used so far seem not to be sufficient to resolve this puzzle.

To this end, we combine STM on a semiconducting surface with Kelvin probe force spectroscopy (KPFs) [14], which allows an independent and direct measurement of the CPD, which fixes the polarity of  $\text{TIBB}(V)$  for all voltages. With this combination, we revisit the shallow acceptor Zn buried in GaAs [9, 11, 12, 15, 17]. Our method reveals that the enhanced conductance induced by shallow acceptors is not only present in one single band-bending regime, as argued in previous publications [9, 11, 12], but *similarly* in the regimes of negative, zero, and positive  $\text{TIBB}(V)$ .

The spatially localized band bending in an STM setup will split off the foremost acceptor state from an impurity band. In the most simple picture [9, 11, 12], this state was treated as being isolated. However, for small  $\text{TIBB}(V)$ , this state is still part of the delocalized impurity band, and only with increasing  $\text{TIBB}(V)$  is it gradually becoming split off and isolated. The increasing localization of the state will affect its charging energy, which may become relevant when considering charge transport. Hence, not only  $\text{TIBB}(V)$  itself but also the *effective* electronic coupling and the charging energy of the acceptor state change with increasing bias voltage during spectra acquisition. Additionally, the band bending will

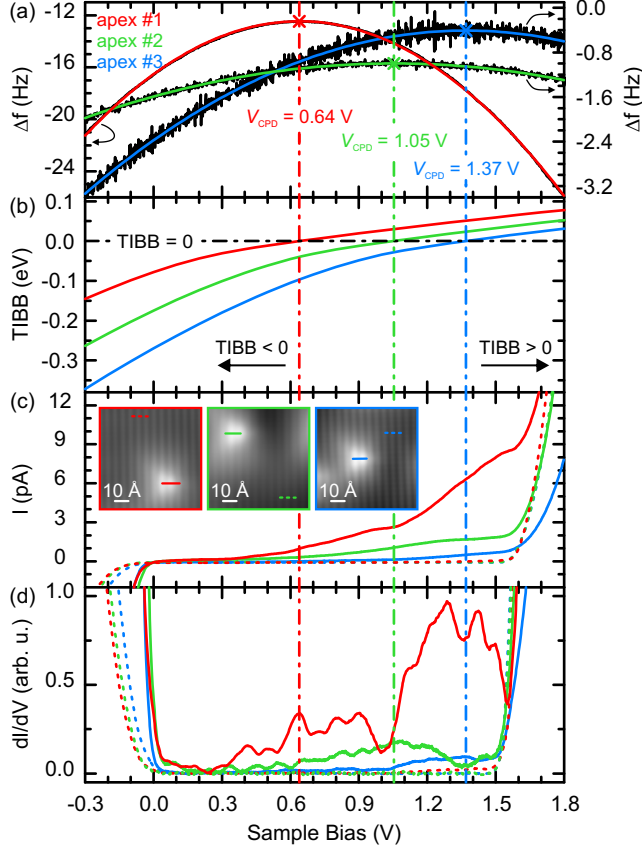


FIG. 1. Contact potential difference and acceptor-induced conductance for different tip apices. (a) Frequency shifts measured as a function of sample bias  $\Delta f(V)$  (black lines), parabolic fits, and the corresponding flat-band voltages  $V_{\text{CPD}}$  are indicated (colored lines). (b) Calculated tip-induced band bending. For any sample bias below (above)  $V_{\text{CPD}}$ , the band bending is negative (positive). (c),(d) show  $I(V)$  and  $dI/dV(V)$  spectra away from (dashed lines) and atop (solid lines) sub-surface acceptors, positions are indicated in the constant-current STM images (inset:  $V = 1.5$  V,  $I = 20$  pA). For all tip apices, acceptor-induced enhanced current and conductance are observed in negative, zero, and positive band-bending regimes.

affect more than just a single acceptor. Accordingly, we treat the electronic transport within the junction using an Anderson-Hubbard model for the foremost acceptor states which are affected by  $\text{TIBB}(V)$ .

Experiments were performed by means of a combined STM and atomic force microscope, which was operated in ultrahigh vacuum at a temperature of  $\sim 5$  K, using a qPlus force sensor equipped with a Pt/Ir tip [17]. As samples, we use commercially available GaAs

wafers, which are cleaved *in situ* to expose the (110) surface. The samples are *p* type doped with Zn, at an average dopant concentration of  $1 \times 10^{19} \text{ cm}^{-3}$ , which establishes an impurity band of 24 meV width, centered around 31 meV above the valence-band edge [8]. This concentration corresponds to an average nearest-neighbor acceptor distance of  $\approx 45 \text{ \AA}$  and a penetration depth of the field of roughly twice this length [19]. Assuming a tip radius of  $\gtrsim 150 \text{ \AA}$ , we expect about ten acceptors to be located within the TIBB-induced space-charge region [20].

Figure 1 shows STM and KPFS measurements performed with three different tip apices. These have been changed by controlled indentation into a clean Cu(111) surface. In the following, we will discuss data acquired with tip apex #1 (red lines in Fig. 1) while showing the results for three different tip apices to underscore the general validity of our findings. Figure 1(a) shows KPFS data. In KPFS, the frequency shift  $\Delta f(V)$  of the force sensor is recorded as a function of the dc sample bias  $V$  at a fixed tip position. The electrostatic contribution to the force between tip and sample gives rise to a parabolic dependence of  $\Delta f(V)$  with  $V$  as  $\Delta f(V) \propto -(V - V_{\text{CPD}})^2$  [21]. For compensated CPD, that is, for  $V = V_{\text{CPD}}$ , the electrostatic field in the tip-sample junction will be zero and  $\Delta f(V)$  will be maximal, respectively. In this situation, there is no electric field to penetrate the semiconductor and hence  $V_{\text{CPD}}$  is the flat-band voltage [22]. From the parabolic fit to  $\Delta f(V)$  [cf. Fig 1(a)], we extract a flat-band voltage of +0.64 V for tip apex #1 [23]. The assignment of  $V_{\text{CPD}}$  to the flat-band condition relies on the GaAs(110) surface not being subject to Fermi-level pinning, our cleaved surface being atomically flat, and our sample being homogeneous and well conducting at 5 K. As this assignment is the key to our experiments, its uncertainty was quantified as follows. (i) Performing KPFS on GaAs at a set of different tip-sample distances showed that local variations of the work function [24] of the tip apices used contribute to this uncertainty only by about  $\pm 30 \text{ meV}$ , and (ii) we measured  $V_{\text{CPD}}$  values on GaAs(110) and on clean Cu(111) with the same tip apices and compared the differences to the values expected from literature [20]. This provides a generous upper bound for the uncertainty of the absolute value of  $V_{\text{CPD}}$  of 0.12 eV [25, 26], which is still small compared to the voltage scales considered here. Finally, we note that tunneling current vs tip-sample distance [ $I(z)$ ] spectra acquired additionally do not result in correct or self-consistent CPD values [14, 20].

As  $\text{TIBB}(V)$  is a monotonic function of the applied sample bias, shifted with respect to zero bias by the CPD, we can attribute a negative (positive)  $\text{TIBB}(V)$  to any sample bias

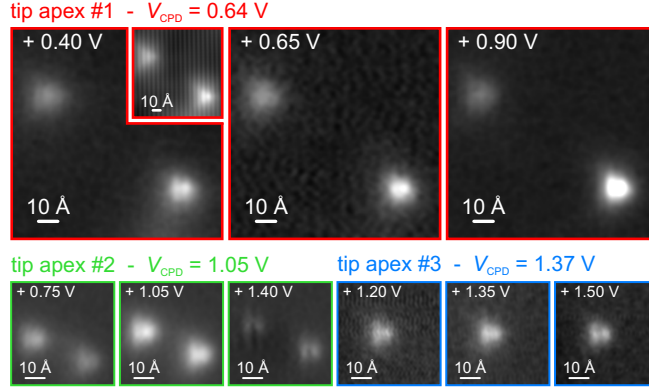


FIG. 2.  $dI/dV$  maps of subsurface acceptors acquired with tip apices #1 (inset: constant-current topography,  $V = 1.5$  V,  $I = 20$  pA) to #3. For each apex, maps are acquired at voltages below, at, and above the corresponding flat-band voltage (sample biases as indicated; the gray scale is identical for each apex). For all apices, within all band-bending regimes, a similar triangular feature of enhanced conductance is observed.

below (above)  $+0.64$  V, and  $\text{TIBB}(0.64 \text{ V}) = 0$  for tip apex #1. The voltage dependence of  $\text{TIBB}(V)$  is shown in Fig. 1(b), where we used  $V_{\text{CPD}}$  as an input parameter to a one-dimensional Poisson-equation solver developed by Feenstra [28]. The flat-band voltage [and the corresponding zero crossing of  $\text{TIBB}(V)$ ] is indicated by a vertical (horizontal) dash-dotted line. We point out that the magnitude of  $\text{TIBB}(V)$  is still uncertain, as it depends on the geometry of the tip, which cannot be easily extracted from KPFS.

Now, we investigate the electronic transport through Zn acceptors buried below the GaAs(110) surface by means of STS in view of the experimentally determined CPD for tip apex #1. Figures 1(c) and 1(d) show (spatially averaged)  $I(V)$  and differential conductance [ $dI/dV(V)$ ] spectra, recorded away from and atop a subsurface acceptor, as is indicated by the colored lines in the constant-current topography shown in the inset. Both spectra show  $p$ -type semiconducting characteristics, with a valence-band-related current onset below 0 V and a conduction-band-related current onset above 1.5 V. In contrast to the spectra as acquired away from the acceptor, the spectra acquired atop the Zn acceptor also show nonzero current and conductance within a large bias interval located within the semiconducting band gap. Whereas this has been reported before [9, 11, 12], the nonzero conductance has so far never been related to quantitative contact potential difference measurements. For this particular tip apex the flat-band condition has been unambiguously determined to be  $+0.64$  V;

therefore we immediately see that acceptor-related conductance is present for negative, zero, and positive TIBB( $V$ ). The same holds true for data acquired with tip apices #2 and #3 which show distinctly different values of the CPD (1.05 and 1.37 eV, respectively); see Fig. 1.

To map out the spatial dependence of the acceptor-related enhanced conductance, we have recorded differential conductance maps. In Fig. 2, we show  $dI/dV$  maps acquired with tip apices #1 to #3, recorded at bias voltages well below, right at, and well above the corresponding flat-band voltage. In accordance with previous experiments, we observe a triangular feature of enhanced conductance at the position of the dopant atom [11]. Most notably, for all apices, a similar pattern of enhanced conductance is observed for negative, zero and positive band bending. The similarity present in different band-bending regimes suggests that *one* conduction mechanism is responsible for all of them. Most importantly, the polarity of the sample bias of the differential conductance maps for all three band-bending regimes remains the same, such that the occurrence of the same conduction mechanism is not related to bipolar tunneling [10, 11, 29]. The basis of most pictures used so far in this context is a single *isolated* acceptor level being shifted by TIBB( $V$ ) against the Fermi level. In this picture, the occupation of the level has to change when shifted across the Fermi level, which determines whether or not a particular channel can contribute to transport, independent of the further details of the model [9, 12]. Hence, in these pictures, no transport mechanisms can be active in *all* three regimes for one particular sample bias polarity. However, our conductance spectra, related to the flat-band voltage, in combination with the  $dI/dV$  maps, indeed suggest that one conduction mechanism is active in all three regimes.

To resolve this controversy, we treat the system as a linear chain of  $N$  equidistant acceptor states between the microscope's tip and the bulk of the sample; see the inset of Fig. 3(a). In this picture, three energies are important for the description. (i) The band bending shifts the on-site energy  $\epsilon_i$  of each acceptor state, depending on its position below the surface. This shift is zero deep inside the bulk and is assumed to increase quadratically towards the surface, where it reaches TIBB( $V$ ) as plotted in Fig. 1(b). (ii) Adjacent acceptor states are coupled via a hopping parameter  $t$ , which we have taken, in accordance with the impurity band width of about 20 meV, to be  $t = 5$  meV. (iii) In our system, the on-site Coulomb energy  $U$  of an isolated acceptor is estimated to be on the order of 10 meV, given a size of the acceptor state of about 20 Å and a dielectric constant of GaAs of about 13 [30–32]. The

Hamiltonian in the Anderson-Hubbard model reads [33–35]

$$\begin{aligned}
H = & \sum_{i=1}^N \sum_{\sigma} \epsilon_i c_{i\sigma}^{\dagger} c_{i\sigma} - t \sum_{i=1}^{N-1} \sum_{\sigma} \left( c_{i\sigma}^{\dagger} c_{i+1\sigma} + c_{i+1\sigma}^{\dagger} c_{i\sigma} \right) \\
& + U \sum_{i=1}^N \left( c_{i\uparrow}^{\dagger} c_{i\uparrow} - \frac{1}{2} \right) \left( c_{i\downarrow}^{\dagger} c_{i\downarrow} - \frac{1}{2} \right)
\end{aligned}$$

where  $c_{i\sigma}^{\dagger}$  creates and  $c_{i\sigma}$  annihilates an electron of spin  $\sigma$  on the  $i$ th acceptor. Here, we choose  $N = 5$  [20]. The rest of the acceptor states and the valence and the conduction bands have been modeled as an electron bath with the respective densities of states. The metallic tip has been treated analogously, having a constant density of states. Further, we assume that the tunneling between tip and acceptors is restricted to the most superficial acceptor [cf. the inset of Fig. 3(a)]. All foremost acceptors are coupled to the bulk of the sample. We note that energy dissipation is expected to occur via the inelastic excitation of vibrons [36]. The dynamics of the system is understood as a sequence of tunneling events from (to) the tip or the bulk of the sample which increase (reduce) by 1 the number of electrons populating the foremost acceptors. The method of choice for the description of these sequential tunneling dynamics is thus the master equation approach [20]. In accordance with the experimental situation, the tunneling rate  $\Gamma^T$  to and from tip states is by far the smallest, and thus the foremost acceptors are essentially in equilibrium with the bulk. Moreover, for  $V \approx V_{\text{CPD}}$ , electrons cannot tunnel from the foremost acceptors to the tip since all transport resonant levels lie far below the tip's Fermi level. Under these assumptions, the current through the system takes the form  $I = e\Gamma^T (2 - \langle n_N \rangle)$ , where  $\langle n_N \rangle$  is the average occupation of the most superficial acceptor [see Fig. 3(b)].

This many-body approach ensures that the *gradual change* of (i) the effective electronic coupling, (ii) the localization, and (iii) the charging energy of the relevant states as a function of bias voltage is inherently captured. Figure 3(a) shows the simulated  $I(V)$  and  $dI/dV(V)$  spectra for different values of  $U$ . Neglecting charging energy ( $U = 0$ ), it shows enhanced current and conductance within a large bias range in different band-bending regimes, for one sample bias polarity only, which is in accordance with our experimental findings. This phenomenon can be understood as follows. For  $V \simeq V_{\text{CPD}}$ ,  $\text{TIBB}(V)$  is smaller than the impurity-band width, and hence the foremost acceptor state is still part of the impurity band, even if slightly detuned from the bulk impurity states. In this voltage region, the Fermi level still remains inside this impurity band that extends to the foremost acceptor,

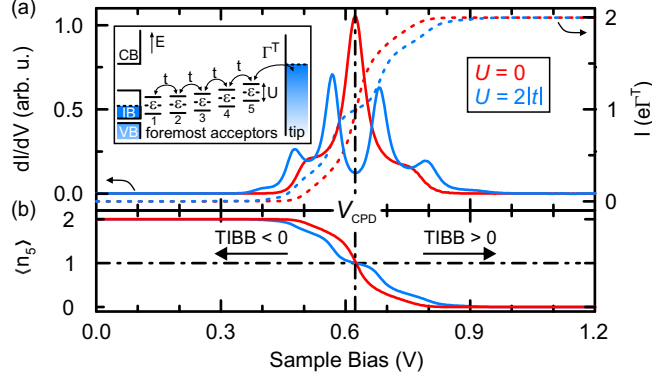


FIG. 3. Simulated electron transport within the junction. (a) Calculated  $I(V)$  (dashed lines) and  $dI/dV(V)$  (solid lines) spectra for vanishing ( $U = 0$ ) and nonvanishing on-site Coulomb energy ( $U = 2|t|$ ). The simulation yields nonzero current and conductance in a broad voltage range including negative, zero, and positive band bending. The inset sketches the relevant energies of the single-particle levels used as input for the many-body calculations. (b) Calculated average population  $\langle n_5 \rangle$  of the foremost acceptor.

and hence, finite conductance is observed. The size of this bias voltage range around  $V_{CPD}$  is given by the impurity-band width  $4t$  divided by the lever arm  $\alpha = \text{TIBB}(V)/V$ . For  $U \neq 0$ , several peaks and dips appear in the spectra as opposed to just a single broad peak that is observed for  $U = 0$ . Close to  $V_{CPD}$ , the single occupation of the foremost acceptor prevails until  $|\text{TIBB}(V)|$  overcomes  $U/2$ . Hence, the average population and the current develop a plateau around  $V_{CPD}$  of width  $U$  divided by  $\alpha$ . Slight modifications in the on-site energies  $\epsilon_i$  and in the tunneling coupling  $t_{ij}$  between adjacent states  $i$  and  $j$  result in variations of the relative peak heights as well as their positions with respect to  $V_{CPD}$  [20].

The simulated spectra in Fig. 3(a) are in qualitative agreement with our experimental ones [37], showing enhanced conductance in all three band-bending regimes. The experimental spectra show enhanced conductance over an even wider bias range than our theory predicts. Whereas  $U$  and  $\alpha$  may differ from the values anticipated here, we note that electron-vibration coupling [36] could also play an important role, the incorporation of which goes beyond the scope of our model.

Finally, we note that the knowledge of the CPD in our experiments also sheds new light onto the interpretation of the observation of charge density oscillations around acceptors [17], as is discussed in the Supplemental Material [20].



In summary, the use of combined STS and KPFS allows us to unambiguously relate the conductance properties of shallow acceptors buried in GaAs to the energy scale of the system, by measuring the flat-band voltage. These measurements show that the voltage range of enhanced acceptor-induced conductance spans three different band-bending regimes, ruling out previous conceptions of electronic transport used in this context [9, 11, 12]. This experimental finding requires a theoretical description which inherently captures the crossover between the acceptor state being part of an impurity band for zero band bending, and the acceptor state being split off and localized for strong negative or positive band bending, respectively. Transport calculations based on an Anderson-Hubbard model yield spectra in qualitative agreement with our experiments. We expect that this combination of Kelvin probe and scanning tunneling spectroscopy can shed new light on the energetics in cross-sectional STM experiments far beyond the specific model system studied here.

The authors thank S. Rolf-Pissarczyk, D. Gohlke, F. J. Gießibl, and M. Morgenstern for valuable discussions and M. Utz, M. Neu, and A. Pöllmann for instrumentation support. Funding from the Volkswagen Foundation (Lichtenberg Program) and the Deutsche Forschungsgemeinschaft (SFB 689, SPP 1243, and SPP 1285) is gratefully acknowledged.

- 
- [1] R. M. Feenstra and J. A. Stroscio, *J. Vac. Sci. Technol. B* **5**, 923 (1987).
  - [2] M. McEllistrem, G. Haase, D. Chen, and R. J. Hamers, *Phys. Rev. Lett.* **70**, 2471 (1993).
  - [3] J. K. Garleff, A. P. Wijnheijmer, and P. M. Koenraad, *Semicond. Sci. Technol.* **26**, 064001 (2011).
  - [4] F. Marczinowski, J. Wiebe, J.-M. Tang, M. E. Flatté, F. Meier, M. Morgenstern, and R. Wiesendanger, *Phys. Rev. Lett.* **99**, 157202 (2007); F. Marczinowski, J. Wiebe, F. Meier, K. Hashimoto, and R. Wiesendanger, *Phys. Rev. B* **77**, 115318 (2008).
  - [5] K. Teichmann, M. Wenderoth, S. Loth, R. G. Ulbrich, J. K. Garleff, A. P. Wijnheijmer, and P. M. Koenraad, *Phys. Rev. Lett.* **101**, 076103 (2008).
  - [6] D. H. Lee and J. A. Gupta, *Science* **330**, 1807 (2010).
  - [7] H. Zheng, J. Kröger, and R. Berndt, *Phys. Rev. Lett.* **108**, 076801 (2012).
  - [8] S. R. Schofield, P. Studer, C. F. Hirjibehedin, N. J. Curson, G. Aeppli, and D. R. Bowler, *Nat. Commun.* **4**, 1649 (2013).

- [9] R. Dombrowski, C. Steinebach, C. Wittneven, M. Morgenstern, and R. Wiesendanger, *Phys. Rev. B* **59**, 8043 (1999).
- [10] K. Hashimoto, C. Sohrmann, J. Wiebe, T. Inaoka, F. Meier, Y. Hirayama, R. A. Römer, R. Wiesendanger, and M. Morgenstern, *Phys. Rev. Lett.* **101**, 256802 (2008).
- [11] G. Mahieu, B. Grandidier, D. Deresmes, J. P. Nys, D. Stievenard, and Ph. Ebert, *Phys. Rev. Lett.* **94**, 026407 (2005).
- [12] S. Loth, M. Wenderoth, L. Winking, R. G. Ulbrich, S. Malzer, and G. H. Döhler, *Phys. Rev. Lett.* **96**, 066403 (2006); S. Loth, M. Wenderoth, R. G. Ulbrich, S. Malzer, and G. H. Döhler, *Phys. Rev. B* **76**, 235318 (2007).
- [13] A. P. Wijnheijmer, J.K. Garleff, M. A. v. d. Heijden, and P. M. Koenraad, *J. Vac. Sci. Technol. B* **28**, 1086 (2010).
- [14] M. Nonnenmacher, M. P. O’Boyle, and H. K. Wickramasinghe, *Appl. Phys. Lett.* **58**, 2921 (1991).
- [15] Z. F. Zheng, M. B. Salmeron, E. R. Weber, *Appl. Phys. Lett.* **64**, 1836 (1994).
- [16] R. de Kort, M. C. M. M. van der Wielen, A. J. A. van Roij, W. Kets, and H. van Kempen, *Phys. Rev. B* **63**, 125336 (2001); R. de Kort, W. Kets, and H. van Kempen, *Surf. Sci.* **482**, 495 (2001).
- [17] F. J. Giessibl, *Appl. Phys. Lett.* **76**, 1470 (2000).
- [18] E. F. Schubert, *Doping in III-V Semiconductors* (Cambridge University Press, Cambridge, England, 1993), p. 23, p. 44 and p. 186.
- [19] R. M. Feenstra, *J. Vac. Sci. Technol. B* **21**, 2080 (2003).
- [20] See Supplementary Material for details on the experimental setup, on the determination of the uncertainty of KPFS, for a comparison of KPFS with  $I(z)$ -spectra, for a detailed description of the Anderson-Hubbard model, and for a discussion of charge density oscillations around acceptors.
- [21] *Kelvin Probe Force Microscopy*, edited by S. Sadewasser and Th. Glatzel (Springer, Heidelberg, 2011), Vol. 48, p. 11 and p. 134.
- [22] Y. Rosenwaks, R. Shikler, Th. Glatzel, and S. Sadewasser, *Phys. Rev. B* **70**, 085320 (2004).
- [23] The standard deviations are below 7 mV.
- [24] F. Krok, K. Sajewicz, J. Konior, M. Goryl, P. Piatkowski, and M. Szymonski, *Phys. Rev. B* **77**, 235427 (2008).

- [25] Ch. Sommerhalter, Th.W. Matthes, Th. Glatzel, A. Jäger-Waldau, and M. Ch. Lux-Steiner, *Appl. Phys. Lett.* **75**, 286 (1999).
- [26] W. Melitz, J. Shen, S. Lee, J. S. Lee, A. C. Kummel, R. Droopad, and E. T. Yu, *J. Appl. Phys.* **108**, 023711 (2010).
- [27] T. König, G. H. Simon, H.-P. Rust, and M. Heyde, *J. Phys. Chem. C* **113**, 11301 (2009).
- [28] The calculation was performed using the SEMITIP software, Version 6, [www.andrew.cmu.edu/user/feenstra/](http://www.andrew.cmu.edu/user/feenstra/), using a absolute tip-sample distance of 10 Å.
- [29] S.W. Wu, G.V. Nazin, X. Chen, X. H. Qiu, and W. Ho, *Phys. Rev. Lett.* **93**, 236802 (2004).
- [30] S. Adachi, *GaAs and Related Materials* (World Scientific, Singapore, 1999), p. 115.
- [31] H. Kamimura and H. Aoki, *The Physics of Interacting Electrons in Disordered Systems* (Oxford University Press, Oxford, England, 1989), p. 2.
- [32] N. F. Mott and E. A. Davis, *Electronic Processes in Non-Crystalline Materials* (Clarendon, Oxford, England 1979), p. 105.
- [33] P. W. Anderson, *Phys. Rev.* **124**, 41 (1961).
- [34] J. Hubbard, *Proc. R. Soc. London, Ser. A* **276**, 238 (1963).
- [35] P. I. Arseev, N. S. Maslova, V. I. Panov, and S. V. Savinov, *J. Exp. Theor. Phys.* **94**, 191 (2002).
- [36] M. Berthe et al., *Phys. Rev. Lett.* **97**, 206801 (2006).
- [37] We note that a non-constant tip density of states may influence experimental  $I(V)$  spectra. To avoid such influence, we prepared metal-terminated apices on Cu(111) before taking spectra on GaAs.

## SUPPLEMENTAL MATERIAL

In this supplemental material, we present details on the experimental setup and on the determination of the uncertainty of the KPFS measurement. A comparison of CPD values as inferred from  $I(z)$ -spectroscopy and as determined from KPFS is provided. Further, we present data on the bias dependence of the onset of local density of states oscillations around acceptors. Finally, a detailed description of the Anderson-Hubbard model is presented.

### Experimental Setup

In our setup, the bias voltage  $V$  is applied to the sample with respect to the microscope's tip. The contact resistance between the GaAs sample and the sample-holder was found to be in the  $k\Omega$  range, at a temperature of 5 K, which is many orders of magnitude below the resistance of the tunnel junction.

To record all current  $I$  versus  $V$  spectra and differential conductance ( $dI/dV$ ) maps at the same absolute tip height above the GaAs(110) surface, we first opened the feedback loop of the STM at  $V = 1.8$  V,  $I = 20$  pA, with tip located away from acceptors, and then moved the tip to the position where spectra or  $dI/dV$  maps were taken. For  $dI/dV$  maps acquired with tip apex #2, the tip-sample distance was decreased by  $\Delta z = 0.25$  Å once the feedback-loop of the STM was interrupted.  $I(V)$  spectra are (except where stated otherwise) averaged over each 10 single spectra, acquired along a line in a specific sample region.  $dI/dV(V)$  spectra are numerically derived from the  $I(V)$  data, data points are averaged over a bias range of 50 mV. For  $dI/dV$  maps, we used lock-in technique with 50 mV peak-to-peak at 166 Hz.

For KPFS, the tip was retracted by  $\Delta z = 5$  Å once the feedback-loop of the STM was interrupted at  $V = 1.8$  V,  $I = 20$  pA. For such increased distance, the CPD measurement is not influenced by atomic-scale variations of the sample surface, but depends only on the long-range electrostatic interaction between tip and sample [1]. Moreover, at such increased distance, the tunneling current is zero, such that we can exclude any influence of the current on the  $\Delta f(V)$  signal [2]. As oscillation amplitudes ( $A$ ) of the qPlus force sensor (spring constant ( $k$ )  $\approx 1.8 \times 10^3$  N/m<sup>-1</sup>, resonance frequency ( $f_0$ )  $\approx 26$  kHz, quality factor ( $Q$ )  $\approx 10^4$ ), we used 1.2 Å, 2.5 Å, and 0.5 Å for measurements with tip apices #1, #2, and #3, respectively.

The apex of the microscope’s tip was treated by controlled indentations into the (111) surface of a Cu single crystal. The Cu single crystal, mounted on a dual sample-holder next to the GaAs sample, was prepared by repeated sputter and annealing cycles, which were performed prior to the GaAs cleavage.

To ensure that the apex of the microscope’s tip used to probe the GaAs(110) surface is identical to that for the Cu(111) surface, the relative alignment between both planar surfaces has been adjusted to be accurate within  $3^\circ$ . To test whether the tip apex was indeed the same when probing both surfaces, we transferred a CO molecule to the apex on one surface and moved the tip over to the other sample surface. There we observed the high lateral resolution that can be attributed to a CO-functionalized tip.

### Kelvin probe force spectroscopy for different tip-sample distances

KPFS measurements can be subject to averaging effects, if areas of different work function contribute to the measurement [3]. As our sample is atomically flat and homogeneous, such artifacts can arise only if the work function of the tip is spatially inhomogeneous. If this is the case, the measured contact potential difference (CPD) is a weighted average over different tip regions of different work functions. As in KPFS the ratio of contribution of

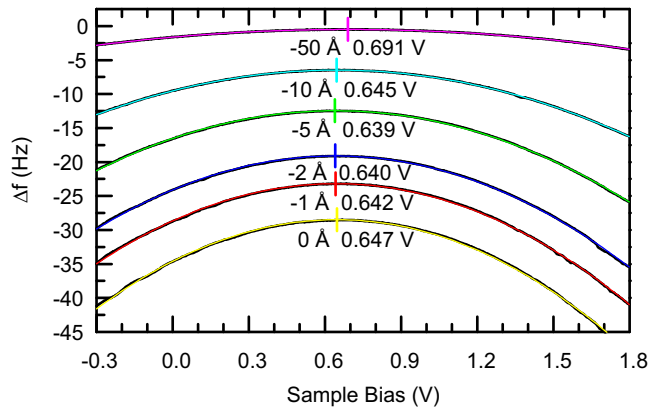


FIG. 4. KPFS for different tip-sample distances. The frequency shifts  $\Delta f(V)$  (black) are fitted by Kelvin parabolas (colored). The standard deviation of each fit is below 1 mV. The relative tip-sample distances  $\Delta z$  and the corresponding contact potential differences  $V_{CPD}$  are indicated below each curve. The total variation of  $V_{CPD}$  is very small compared to sample bias range considered in our experiment.

different parts of the tip strongly depends on their relative distance to the sample, such inhomogeneity would result in different values for the CPD measured for different absolute tip-sample distances [3]. Figure S4 shows KPFS measurements for different absolute tip-sample distances acquired with tip apex #1. At a setpoint of  $V = 1.8$  V and  $I = 20$  pA the feedback-loop of the STM was opened. The tip was then retracted by different values of  $\Delta z$  ranging from 0 to 50 Å, and  $\Delta f(V)$  was recorded. We find the peak positions of the Kelvin parabolas to differ by less than 45 mV in total. For tip apices #2 and #3 we proceeded likewise, finding total variations of below 23 mV and 52 mV, respectively. This variation of the CPD for individual apices is very small compared to the bias voltage range considered here. Accordingly, for the tip apices used, inhomogeneities can be largely ruled out, and we expect the error of  $V_{\text{CPD}}$  from this side to be on the order of a few 10 meV.

### Determination of the absolute error of the KPFS measurements

To determine the absolute experimental uncertainty of our KPFS measurements on GaAs(110), we used KPFS data acquired on the clean Cu(111) surface (used for tip preparation) as a reference. For an individual tip apex, we determined the voltage corresponding to the CPD on both surfaces, *i.e.*  $V_{\text{CPD}}^{\text{GaAs}}$  and  $V_{\text{CPD}}^{\text{Cu}}$  [4, 5]. Figure S5 shows, for eight individual tip apices (with tip work functions varying by 0.4 eV),  $\Delta V_{\text{CPD}} = V_{\text{CPD}}^{\text{GaAs}} - V_{\text{CPD}}^{\text{Cu}}$ . In total,

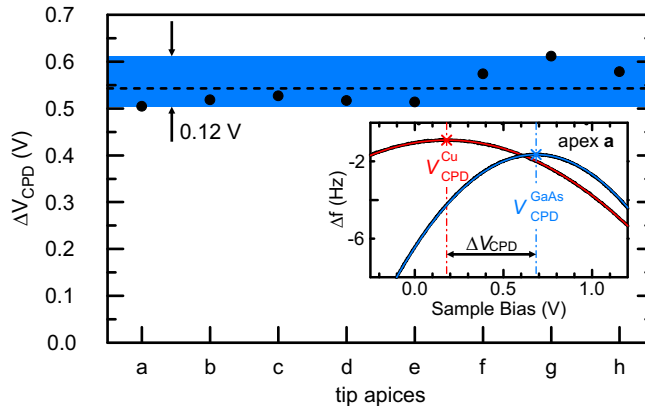


FIG. 5. Difference of the contact potential difference acquired on Cu(111) and on GaAs(110),  $\Delta V_{\text{CPD}}$ , for eight individual tip apices. The horizontal dashed line indicates the arithmetic average of  $\Delta V_{\text{CPD}}$  (0.54 V), its absolute variation is found to be 0.12 V. The inset shows, as an example,  $\Delta f(V)$  data acquired with tip apex **a** (black lines), parabolic fits are indicated (colored).

$\Delta V_{\text{CPD}}$  is found to vary by 0.12 V, at an arithmetic averaged value of 0.54 V. From the literature,  $\Delta V_{\text{CPD}}$  is expected to be

$$\begin{aligned}\Delta V_{\text{CPD}} &= \frac{1}{e} [\chi_{\text{GaAs}(110)} + (E_C - E_F) - \phi_{\text{Cu}(111)}] \\ &= 4.07 \text{ V} + 1.49 \text{ V} - 4.94 \text{ V} \\ &= 0.62 \text{ V}\end{aligned}\tag{1}$$

with  $\chi_{\text{GaAs}(110)}$  and  $(E_C - E_F)$  being the electron affinity of GaAs(110) and the difference between conduction band edge and Fermi-level in Zn-doped GaAs, respectively, and  $\phi_{\text{Cu}(111)}$  being the work function of the clean Cu(111) surface. From the literature, we have taken 4.94 eV for the work function of Cu(111) [6], 4.07 eV for the electron affinity of GaAs(110) [7], and  $(1.52 - 0.03) \text{ eV} = 1.49 \text{ eV}$  for the energetic difference between conduction band edge and Fermi-level in Zn-doped GaAs, with the Fermi-level located 0.03 eV above the edge of the valence band [7, 8].

Accordingly, we estimate the absolute error of the voltage corresponding to the flat-band condition,  $V_{\text{CPD}}$ , as extracted from KPFS on GaAs(110), to be below 0.12 V, which is small compared to the voltage scale of interest.

### Comparison of $I(z)$ -spectroscopy and KPFS

In the literature, in the context of acceptor-induced enhanced conductance, the dependence of the tunneling-current  $I$  on tip-sample distance  $z$  was used to infer the CPD [9–12]. Figure S6 shows a semi-logarithmic plot of  $I(z)$ -spectra, acquired with tip apex **a** (see inset of Fig. S5 for corresponding  $\Delta f(V)$  data) on Cu(111) and on GaAs(110). On Cu(111), the feedback loop of the STM was interrupted at a current of 2.5 pA and a sample bias of +50 mV, while on GaAs(110) the feedback loop was interrupted at a current of 20 pA and a sample bias of +1.6 V.

In  $I(z)$ -spectroscopy, the tunneling current is assumed to decay exponentially with increasing tip-sample distance,  $I \propto \exp(-2\kappa z)$ . The inverse decay length  $\kappa$  is linked to the apparent barrier height  $\bar{\phi}$  by the expression  $\kappa = \sqrt{2m\bar{\phi}/\hbar^2}$ , where  $m$  is the mass of the free electron.

Whereas comparative  $I(z)$ -spectroscopy of different sample areas can provide a qualitative measure for the changes in work function [13], some caution is in order when trying to

quantitatively interpret the inverse decay length  $\kappa$  [14]. On semiconductors, things are expected to be even more complicated, as TIBB( $V$ ) changes also with distance  $z$ , which can additionally affect the  $I(z)$ -spectra, by changing the number of states in the sample available for tunneling. The derivation of an actual value for the CPD from  $I(z)$ -spectra depends strongly on the model for tunneling that is applied [9–12]. For easy comparison, we here use a model solely based on geometrical considerations, which was applied previously by Loth *et al.* [9–11].

On GaAs(110), for  $eV > (E_C - E_F)$ , the apparent barrier height is connected with the tip's work function,  $\phi_{\text{tip}}$ , via [11]:

$$\bar{\phi} = \frac{\chi - [eV - (E_C - E_F)] + \text{TIBB}(V) + \phi_{\text{tip}}}{2} \quad (2)$$

In this equation, TIBB( $V$ ) gives rise to a small correction (below 0.1 eV, c.f. Fig. 1(b), positive sample bias), which is unimportant for our comparison and which we therefore neglect. Solving equation 2 for  $\phi_{\text{tip}}$  one can then calculate  $V_{\text{CPD}}^{\text{GaAs(110)}}$  via:

$$V_{\text{CPD}}^{\text{GaAs(110)}} = \frac{1}{e} [\chi + (E_C - E_F) - \phi_{\text{tip}}] \quad (3)$$

On Cu(111), we proceed likewise, connecting the apparent barrier height  $\bar{\phi}$  with the work functions of tip and sample via:

$$\bar{\phi} = \frac{1}{2} (\phi_{\text{tip}} + \phi_{\text{Cu(111)}}) \quad (4)$$

leading to

$$V_{\text{CPD}}^{\text{Cu(111)}} = \frac{2}{e} (\phi_{\text{Cu(111)}} - \bar{\phi}) \quad (5)$$

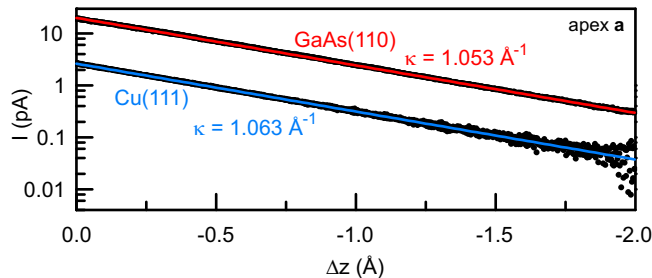


FIG. 6.  $I(z)$ -spectroscopy on Cu(111) and on GaAs(110) surfaces (black, semilogarithmic plot), single-exponential fits and corresponding values of the inverse decay length  $\kappa$  are indicated (color).



	KPFS	$I(z)$
$V_{\text{CPD}}^{\text{Cu}(111)}$ (V)	$0.18 \pm 0.12$	1.27
$V_{\text{CPD}}^{\text{GaAs}(110)}$ (V)	$0.68 \pm 0.12$	1.06

TABLE I. Comparison of  $V_{\text{CPD}}$ , for one individual tip apex, as determined from KPFS and inferred from  $I(z)$ , on Cu(111) and on GaAs(110).

In Table I, we present, for tip apex **a**,  $V_{\text{CPD}}$  as determined from KPFS and as inferred from the  $I(z)$ -spectra shown in Fig. S6.

In addition, for tip apex #3 (main text), we record a series of 20  $I(z)$ -spectra on GaAs(110), equidistant spaced along a 40 Å long line, oriented parallel to the crystallographic [001] direction, located away from dopant atoms or defects. Using the model described above, we inferred  $V_{\text{CPD}}$  from each individual spectra, and subsequently calculate mean and standard deviation of the series of spectra. This procedure was repeated three times, varying the sample bias at which the feedback-loop of the STM was interrupted at a current of 20 pA. The corresponding results are presented in Table II.

sample bias (V)	KPFS	$I(z)$		
		+1.5	+1.6	+2.0
$V_{\text{CPD}}^{\text{GaAs}(110)}$ (V)	$1.37 \pm 0.12$	$0.65 \pm 0.43$	$-0.01 \pm 0.30$	$1.81 \pm 0.14$

TABLE II. Comparison of  $V_{\text{CPD}}$ , as determined from KPFS and inferred from  $I(z)$ -spectroscopy for tip apex #3.  $I(z)$ -spectroscopy was performed for three different setpoint-values of the sample bias.

The above analysis shows that the CPD values derived from  $I(z)$ -spectroscopy are neither consistent with the differences in work function for Cu(111) and GaAs(110) as known from the literature nor are self-consistent, when comparing data acquired at different sample biases. We note that the difference in CPD between Cu(111) and GaAs(110) as derived from  $I(z)$ -spectroscopy even has the wrong sign.

Finally, we note that including mirror charge effects to the model of tunneling, as proposed by Wijnheijmer *et al.*, is expected to considerably lower the flat-band voltage  $V_{\text{CPD}}$  (by  $\sim 1$  eV) [12], which again would not result in correct values for  $V_{\text{CPD}}$ .

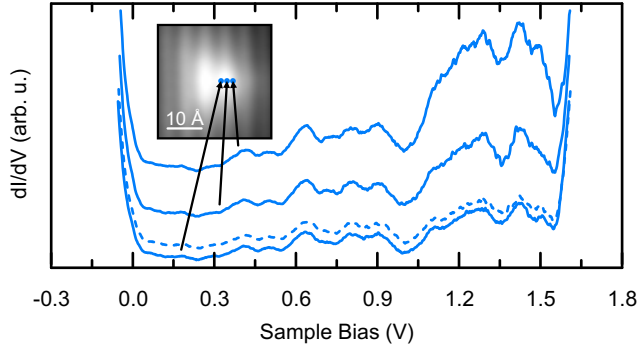


FIG. 7. Spatially resolved  $dI/dV(V)$  spectra acquired atop a subsurface acceptor (inset:  $V = 1.5$  V,  $I = 20$  pA). Three spectra (solid lines) were acquired at three different sample positions very close to one another. The spectra are vertically offset for clarity. At the same position of the lowest of these spectra, an additional spectrum (dashed line) was acquired.

### Spatially resolved $dI/dV(V)$ -spectra

In the main text, in Fig. 1(c) we show (numerically derived)  $dI/dV(V)$  spectra, spatially averaged over 10 single spectra, acquired along a line at a specific sample region. To prove the reproducibility of our data, in Fig. S7 we show four individual, spatially resolved (numerically derived)  $dI/dV(V)$  spectra (vertically offset for clarity), acquired with tip apex #1. The two lowest (dashed and solid) were acquired at the same position, whereas the others were taken after slightly moving the tip laterally as indicated in the inset. The spectra acquired at the same position are almost identical, the others continuously evolve while moving the tip laterally. Whereas this clearly demonstrates the high reproducibility of our data, it is still likely that some part of the fine structure of the spectra is related to a non-constant tip density of states. To minimize the latter influence in our spectra, we used a dual sample tip holder in our experiments, which allowed us to prepare a metal-terminated tip on Cu(111) before moving to the semiconductor and taking spectra there.

### Local density of states oscillations

Figure S8 shows two sets of bias-dependent  $dI/dV$  maps acquired with two different tip apices, namely tip apex #1 and an additional tip apex, labeled #4 [15]. The images acquired with tip apex #1 are recorded on the same area as those shown in Fig. 2, main text.

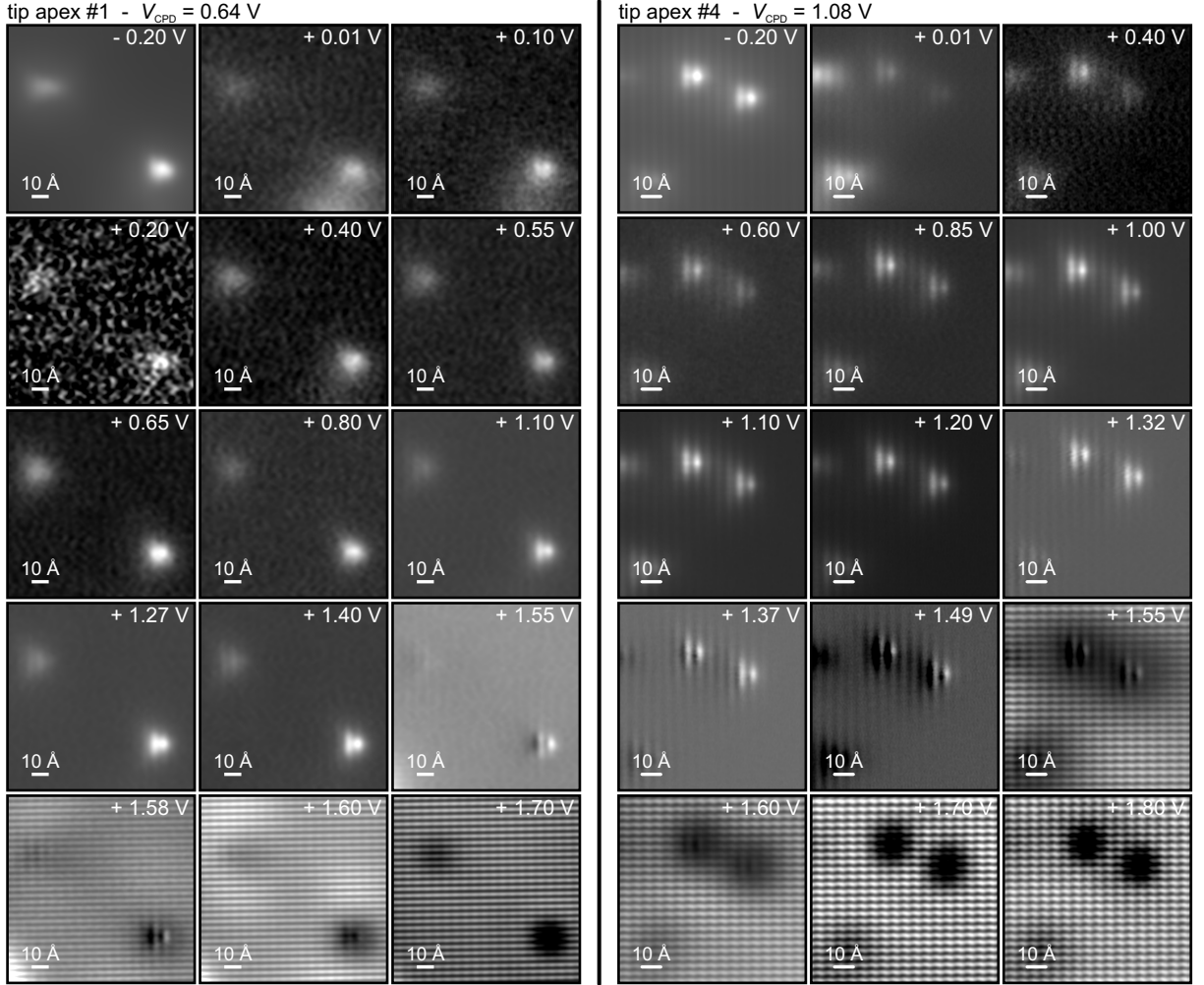


FIG. 8.  $dI/dV$  maps (sample biases as indicated), acquired with two different tip apices #1 (left) and #4 (right), with markedly different flat-band voltages of 0.64 eV and 1.08 eV, respectively. For both apices, within a large sample bias window, including positive sample biases below, at, and above the flat-band voltage, a triangular feature of enhanced conductance is observed at the position of the dopant atoms. Local density of states oscillations are, for both apices, observed only at sample biases corresponding to tunneling of electrons from the tip to the conduction band of the sample (*i. e.* for  $V > 1.5 \text{ V}$ ).

First, we notice that for both tip apices, which have distinctly different flat-band voltages of 0.64 V and 1.08 V, respectively, we observe within a large sample bias region (at positive sample bias polarity), for negative, zero and positive band bending a similar feature of enhanced conductance at the position of the dopant atoms. Hence, as already stated in the

main text, the observation of enhanced conductance is independent of the sign of  $TIBB(V)$ . In fact, we note that for both tip apices, the large sample bias region spans almost the entire semiconductor's band gap region ( $0 < V < +1.52$  V).

Second, we note that for both apices spatial local density of state oscillations are observed *only* for sample biases for which tunneling of electrons from the tip into the conduction band of the sample is possible, *i. e.* for  $V > +1.5$  V. Indeed, for both tip apices those oscillations basically occur at the same sample bias as the checker-board-like corrugation known to be related to tunneling into the conduction band (*i. e.*, the  $C_3$  surface resonance) [16]. In the literature, those oscillations are referred to as charge density oscillations (CDO) [10, 17, 18], and are expected to occur as soon as holes accumulate below the microscope's tip, *i. e.* for  $V \geq V_{CPD}$ . Those CDO are then explained by the accumulated holes scattering at the core-potentials of the dopant atoms.

From our experiments however, relating the onset-voltage of oscillations in the local density of states to a quantitative value of the flat-band voltage, we conclude: whereas the existence of hole accumulation ( $V \geq V_{CPD}$ ) may play a role, the possibility of tunneling into the conduction band ( $V > +1.5$  V) apparently is a necessary requirement for the observation of local density of states oscillations around acceptors in *p*-type GaAs. We note that our observations are consistent with experimental data found in the literature [10, 17].

Further, we note that, when comparing these two apices #1 and #4 in more detail, one realizes that for tip #1 the occurrence of local density of states oscillations occurs at slightly higher sample biases as compared to tip #4 ( $\Delta V \simeq 30$  mV). This slight shift is consistent with the CPD values extracted from KPFS under the assumption that oscillations are related to tunneling into the conduction band, but inconsistent under the assumption of being only related to the situation of hole accumulation.

In summary, this is yet another example that the unknown CPD in previous experiments resulted in misinterpretation of experimental data [10].

### **Detailed description of the Anderson-Hubbard model**

In our theoretical analysis we distinguish between bulk and foremost acceptors, the latter being the ones closer to the tip and thus more strongly affected by  $TIBB(V)$ . Our tunneling junction is described by the total Hamiltonian:

$$H = H_{\text{acc}} + H_{\text{sub}} + H_{\text{tip}} + H_{\text{tun}} \quad (6)$$

where  $H_{\text{acc}}$  describes the foremost acceptors,  $H_{\text{sub}}$  the rest of the acceptors and the hosting semiconductor (the substrate),  $H_{\text{tip}}$  the tip and finally  $H_{\text{tun}}$  contains the tunneling coupling between acceptors, tip, and substrate.

The Hamiltonian for the  $N$  foremost acceptors includes the Coulomb interaction, as already stated in the main text; it reads:

$$\begin{aligned} H_{\text{acc}} = & \sum_{i=1}^N \sum_{\sigma} \epsilon_i c_{i\sigma}^{\dagger} c_{i\sigma} - t \sum_{i=1}^{N-1} \sum_{\sigma} \left( c_{i\sigma}^{\dagger} c_{i+1\sigma} + c_{i+1\sigma}^{\dagger} c_{i\sigma} \right) \\ & + U \sum_{i=1}^N \left( c_{i\uparrow}^{\dagger} c_{i\uparrow} - \frac{1}{2} \right) \left( c_{i\downarrow}^{\dagger} c_{i\downarrow} - \frac{1}{2} \right) \end{aligned} \quad (7)$$

where  $c_{i\sigma}^{\dagger}$  creates an electron of spin  $\sigma$  on the  $i$ th acceptor state,  $\epsilon_i$  is the on-site energy and  $t$  the hopping parameter. Finally,  $U$  is the on-site Coulomb repulsion. For the hopping parameter we have taken the value of  $t = 5$  meV in accordance with the accepted impurity band width of roughly 20 meV. For the Coulomb repulsion term we have assumed values in the range  $U = 10 - 20$  meV. These values for the on-site Coulomb repulsion are far smaller than the ones of an atom in vacuum due to the much larger size of the impurity states ( $a_B \approx 20$  Å) and the dielectric constant of the hosting semiconductor ( $\epsilon_r \approx 13$ ). The on-site energy of the acceptor  $\epsilon_i$  is the one that is more directly affected by TIBB( $V$ ). We have modeled it as:

$$\epsilon_i = \mu_0 + \left( \frac{i-1}{N-1} \right)^2 \text{TIBB}(V) \quad (8)$$

where  $\mu_0$  is the bulk chemical potential of Zn-doped GaAs. Eq.(8) is written assuming a linear chain of equidistant acceptors and a quadratic drop off of the tip induced electrostatic potential inside the semiconductor. The deepest acceptor ( $i = 1$ ) considered in the model is not affected by the tip, while the energy of the most superficial one ( $i = N$ ) is shifted exactly by TIBB( $V$ ), as plotted in Fig. 1(b) of the main text.

In a one-dimensional model, the penetration depth of the electric field into the interior of the GaAs sample is, for the dopant concentration used, estimated to be about 100 Å [19], whereas the average distance of nearest neighbors of acceptors is about 45 Å. In the experimental (three-dimensional) system, assuming a tip-radius of 15 nm, we expect about

10 acceptors to be located within the space-charge region caused by tip. In our model, due to limitations of computational time, we restricted ourself to a one-dimensional, linear chain of  $N = 5$  acceptors.

Due to the particular form of the Coulomb interaction term, the Hamiltonian (7) is particle-hole symmetric if  $\epsilon_i = 0, \forall i$ . This ensures that, in equilibrium, the number of electrons populating the acceptors is always equal to the number of acceptors, irrespective of the strength of the interaction term  $U$ . The constant terms appearing in the interaction and ensuring particle-hole symmetry are also physically justified as the contribution of the positive ions located at the position of the acceptor states. The latter ensure the charge neutrality of the system and should be taken into account when considering the energy contribution of the Coulomb interaction.

The rest of the acceptors together with the hosting semiconductor have been modeled as a free electron bath with temperature  $T$  and chemical potential  $\mu_S$ . Analogous treatment has been reserved to the tip, to which we have assigned the electrochemical potential  $\mu_0 - eV$  where  $e$  is the electron charge taken with sign. Further, we assume that the tunneling between the tip and the foremost acceptors is restricted to the most superficial one ( $i = N$ ). All foremost acceptors are instead coupled to the substrate. Due to the large distance between the tip and the surface of the semiconductor when compared with the average distance between the acceptors, we have assumed a very asymmetric tunneling coupling of the foremost acceptors to the two “leads”.

The dynamics of the system is understood as a sequence of tunneling events from (to) the tip or the substrate which increase (reduce) by one the number of electrons populating the foremost acceptors. The method of choice for the description of this sequential tunneling dynamics is thus the master equation approach. The latter, when applied to second order in the tunneling coupling  $H_{\text{tun}}$  between the system and the tip (substrate), reduces to the set of rate equations:

$$\begin{aligned} \dot{P}_{ME} = & - \sum_{\chi E'} (R_{ME \rightarrow M+1E'}^{\chi} + R_{ME \rightarrow M-1E'}^{\chi}) P_{ME} \\ & + \sum_{\chi E'} R_{M+1E' \rightarrow ME}^{\chi} P_{M+1E'} + \sum_{\chi E'} R_{M-1E' \rightarrow ME}^{\chi} P_{M-1E'} \end{aligned} \quad (9)$$

where the  $P_{ME}$  is the population of the  $M$ -body eigenstate with energy  $E$  of the Hamiltonian  $H_{\text{acc}}$  given in Eq. (7), and  $\chi = S, T$  indicates the substrate and the tip, respectively. The

many body rates follow from Fermi's golden rule:

$$\begin{aligned}
R_{ME \rightarrow M+1E'}^\chi &= \sum_{\sigma} \sum_{i=1}^N \Gamma_i^\chi(E' - E) |\langle M+1E' | d_{i\sigma}^\dagger | ME \rangle|^2 f^+(E' - E - \mu_\chi) \\
R_{ME \rightarrow M-1E'}^\chi &= \sum_{\sigma} \sum_{i=1}^N \Gamma_i^\chi(E - E') |\langle M-1E' | d_{i\sigma} | ME \rangle|^2 f^-(E - E' - \mu_\chi)
\end{aligned} \tag{10}$$

where  $f^\pm(x) = (e^{\pm x/k_B T} + 1)^{-1}$  are Fermi functions,  $\mu_T = \mu_0 - eV$  and  $\mu_S = \mu_0$  are the electrochemical potentials of tip and substrate respectively, and  $\Gamma_i^\chi$  are the energy dependent single particle tunneling rates defined as:

$$\begin{aligned}
\Gamma_i^S(\Delta E) &= \frac{2\pi}{\hbar} |t_S|^2 D_S(\Delta E) \\
\Gamma_i^T(\Delta E) &= \frac{2\pi}{\hbar} |t_T|^2 D_T \delta_{iN}
\end{aligned} \tag{11}$$

where  $D_\chi$  is the density of states of the  $\chi$  lead which we assume constant for the metallic tip. For what concerns the substrate we have included the energy dependence associated to the impurity band and the valence and conduction band of the hosting semiconductor. Fig. S9 shows a plot of the density of states (DOS) of the substrate, normalized to the DOS at the Fermi energy. The relative weight of the three bands are chosen with respect to the density of acceptors and effective masses. We note that we have chosen the DOS within the bulk band-gap to be non-zero (*c. f.* inset of Fig. S9), to mimic energy dissipation. Such dissipation can occur via inelastic excitation of vibrons [20]. This DOS drops exponentially with increasing energy, reflecting the expected energy dependence of dissipation efficiency. We have tested the robustness of our results against different models of the DOS of the substrate.

The substrate tunneling rate is assumed independent of the acceptor index  $i$  while the tip tunneling rate is limited to the most superficial acceptor ( $i = N$ ). Finally the bare tunneling amplitudes  $t_{S,T}$  between the leads and the system of foremost acceptors is responsible for the strong asymmetry of the setup yielding  $\Gamma^T \ll \Gamma^S$ . Since the smallest tunneling rate sets the scale of the current we can estimate  $\Gamma^T \approx 0.1 \mu\text{eV}$ .

Notice that in the definition of the substrate many-body tunneling rate (see eq. 10) we have performed the sum over the acceptor index  $i$  only *after* taking the square of the many-body matrix element. This approximation destroys any spatial correlation between tunneling events and the associated quantum interference effects. In this context, we note that the network of tunneling couplings between the foremost acceptors and the bulk acceptors is

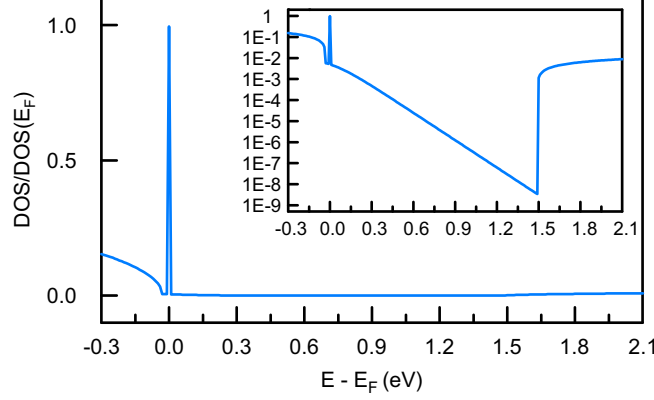


FIG. 9. Density of states of the substrate used in our model (inset: logarithmic plot).

unknown since it depends on the particular acceptor configuration. The approximation applied averages over all these possible configurations, keeping as the only information an average tunneling rate to the entire system of foremost impurities.

The  $I(V)$  characteristics presented in Fig. 3 of the main text are calculated in the stationary limit. They are obtained by solving first the set of equations (9) in the limit  $\dot{P}_{ME} = 0$  and inserting the solution  $P_{ME}^{\text{stat}}$  in the current formulas:

$$\begin{aligned}
I_T &= \sum_{MEE'} M \left[ -(R_{ME \rightarrow M+1E'}^T + R_{ME \rightarrow M-1E'}^T) P_{ME}^{\text{stat}} \right. \\
&\quad \left. + R_{M+1E' \rightarrow ME}^T P_{M+1E'}^{\text{stat}} + R_{M-1E' \rightarrow ME}^S P_{M-1E'}^{\text{stat}} \right] \\
I_S &= \sum_{MEE'} M \left[ -(R_{ME \rightarrow M+1E'}^S + R_{ME \rightarrow M-1E'}^S) P_{ME}^{\text{stat}} \right. \\
&\quad \left. + R_{M+1E' \rightarrow ME}^S P_{M+1E'}^{\text{stat}} + R_{M-1E' \rightarrow ME}^S P_{M-1E'}^{\text{stat}} \right]
\end{aligned} \tag{12}$$

where the (particle) current has been set by convention positive when it increases the number of electrons on the system of foremost acceptors. The stationary limit implies  $I_T = -I_S$ .

The general expression of the current (12) is greatly simplified if  $\mu_T \gg E_{N+1} - E_N$  for every energy and particle number. This condition is experimentally relevant since it is fulfilled if  $V \approx V_{\text{CPD}}$ . In this high bias limit one readily obtains  $R_{ME \rightarrow M-1E'}^T \rightarrow 0$  and, from (12), the current at the tip can be rewritten as:

$$I_T = \sum_{\sigma MEE'} \Gamma_N^T \langle ME | d_{N\sigma} | M+1E' \rangle \langle M+1E' | d_{N\sigma}^\dagger | ME \rangle P_{ME}^{\text{stat}} \tag{13}$$

Since the states with  $M+1$  particle number can be replaced at no prize with a sum over



states with a generic particle number  $M'$ , the current in the high bias limit reads:

$$I_T = \sum_{\sigma MEE'} \Gamma_N^T \langle ME | d_{N\sigma} d_{N\sigma}^\dagger | ME \rangle P_{ME}^{\text{stat}} = \Gamma_N^T (2 - \langle n_N \rangle) \quad (14)$$

where  $\langle n_N \rangle$  is the average population of the most superficial acceptor.

In Fig. 3 (main text) we present the simulation of the current as a function of the sample bias for different strength of the interaction parameter  $U$ . Striking is the appearance, as a function of the interaction strength, of a current plateau around the flat-band condition ( $V = V_{\text{CPD}}$ ). This phenomenon is directly linked to the appearance in the system of a new energy scale, i.e. the on-site Coulomb repulsion: in fact the current is essentially pinned to its flat-band value as far as  $|\text{TIBB}(V)| < U/2$ .

A better understanding of this phenomenon can be obtained by comparing the currents plotted in Fig. 3 (main text) with the acceptors' average occupations and many-body state populations showed in Fig. S10. Both for the vanishing and strong interacting case it is clear that the average occupation of the most superficial acceptor  $\langle n_5 \rangle$  in the left panels of Fig. S10 essentially determines the current through the system: the current is blocked whenever the most superficial acceptor is doubly occupied and the more it flows the lower the average acceptor occupation. In fact, if  $V > 0$  the particle current flows from the tip to the foremost acceptor to the substrate via tip tunneling events which increase by one the electron number on the most superficial acceptor. These events are Pauli blocked for a doubly occupied acceptor, one transport channel ( $| \uparrow \rangle \rightarrow | 2 \rangle$  or  $| \downarrow \rangle \rightarrow | 2 \rangle$ ) opens if  $\langle n_5 \rangle = 1$  and 2 channels ( $| 0 \rangle \rightarrow | \uparrow \rangle$  and  $| 0 \rangle \rightarrow | \downarrow \rangle$ ) for  $\langle n_5 \rangle = 0$ . Finally, it should be noticed that no blocking due to energetic considerations can occur under the approximate flat-band condition  $V \approx V_{\text{CPD}}$ . The system of foremost acceptors is in fact half filled; thus,  $E_{N+1g} - E_{Ng} - \mu_0 \approx U/2$  and a single tip tunneling event can deposit an energy  $|eV_{\text{CPD}}| \gg U/2$  into the system.

The average occupation of the last of the foremost acceptors is strongly influenced by the Coulomb repulsion parameter  $U$ . This influence is best understood by considering the right panels of Fig. S10. Firstly one notices that ground state populations dominates the picture even at extremely large biases ( $V \approx V_{\text{CPD}}$ ). This is due to the combination of low temperature and strong rate imbalance between the tip and the substrate rates. Essentially we can argue that the foremost acceptors are always *in equilibrium* with the substrate. In absence of on-site interaction it does not cost any energy, in the flat-band condition, to

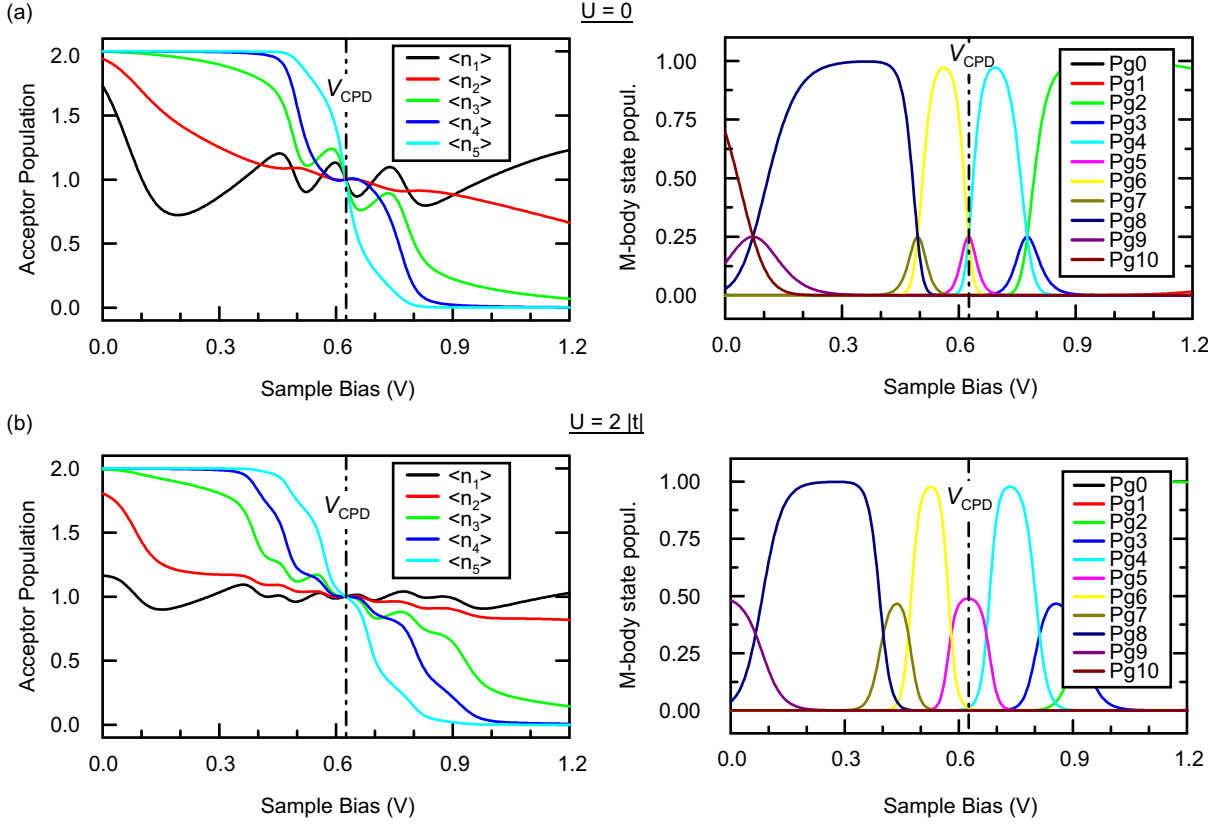


FIG. 10. (a) Left: Plot of the average occupation  $\langle n_i \rangle$  of the 5 foremost acceptors as a function of the sample bias in absence of the on-site Coulomb interaction ( $U = 0$ ). Acceptor 1 is the deepest, acceptor 5 the one closest to the surface. Right: Population of the many-body energy ground states of the 5 foremost acceptors for different particle numbers (Pg), plotted vs. the sample bias. Notice that the ground states with odd particle number are twofold spin degenerate. In each plot, the vertical dashed-dotted line indicates the flat-band voltage. (b) The same as in (a), but for the case  $U = 2|t|$ .

add or remove one electron from the half-filling configuration. This is clearly visible in the right panel of Fig. S10(a) which shows an equal population of 0.25 for the 4-, 5- (2x spin degenerate) and 6-particle ground states [21]. Still in the non interacting case within TIBB( $V$ ) comparable with the impurity bandwidth the 4- (6-) particle ground state reaches full occupation. Most of this change in the particle occupation is concentrating on the last acceptor and correspondingly, on the same energy scale for TIBB( $V$ ), the current saturates (vanishes).

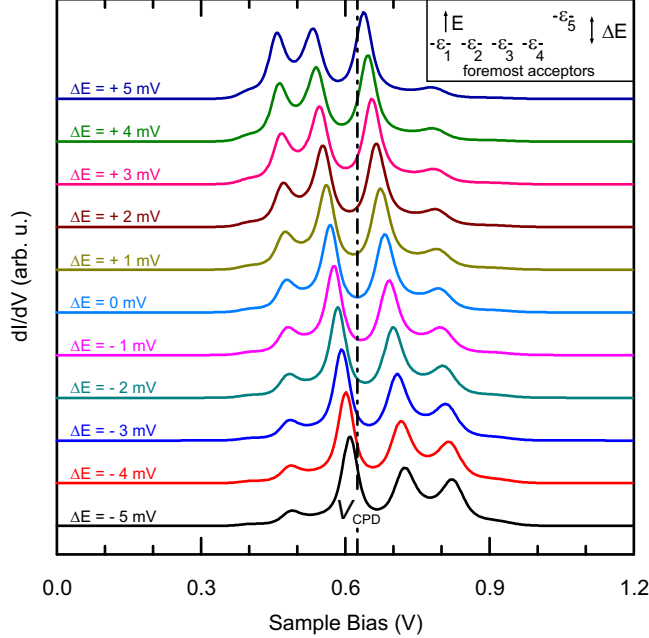


FIG. 11. Calculated  $dI/dV(V)$  spectra, for  $U = 2|t|$ , for eleven different values of the on-site energy of the most superficial acceptor,  $\epsilon_5$  (the inset corresponds to  $\text{TIBB}(V) = 0$ ). The on-site energy is varied in the range  $-5 \text{ meV} \leq \epsilon_5 \leq +5 \text{ meV}$ . The spectra are vertically offset for clarity. Slight variations of the on-site energy result in considerable shifts of the peak positions with respect to the flat-band voltage  $V_{\text{CPD}}$  and in changes of the relative peak heights.

The interaction lifts this degeneracy and the average population of the half-filled ground state develops a plateau of width  $U$  on the scale of  $\text{TIBB}(V)$ , thus approximately  $15|U/e|$  on the bias scale due to level arm scaling. This plateau is readily understood by noticing that the energy needed to add or remove a particle at half filling is exactly  $\Delta E = U/2$ .

Finally, we have tested the results of our theoretical model against variations of different parameters such as: the number of foremost acceptors  $N$ , the temperature  $T$ , the on-site energies  $\epsilon_i$  [22, 23] and the inter-acceptor tunnelling parameter  $t$ . The results are reported in Figs. S11 to S13.

In Fig. S11 we show the differential conductance as a function of the bias voltage. The different curves refer to different values of the on-site energy  $\epsilon_5$  and are shifted for clarity. While the qualitative picture does not change, even slight variations of the on-site energy (on the order of a few meV) result in considerable shifts of the peak position and relative heights in the differential conductance. This is in accordance with experimental results.

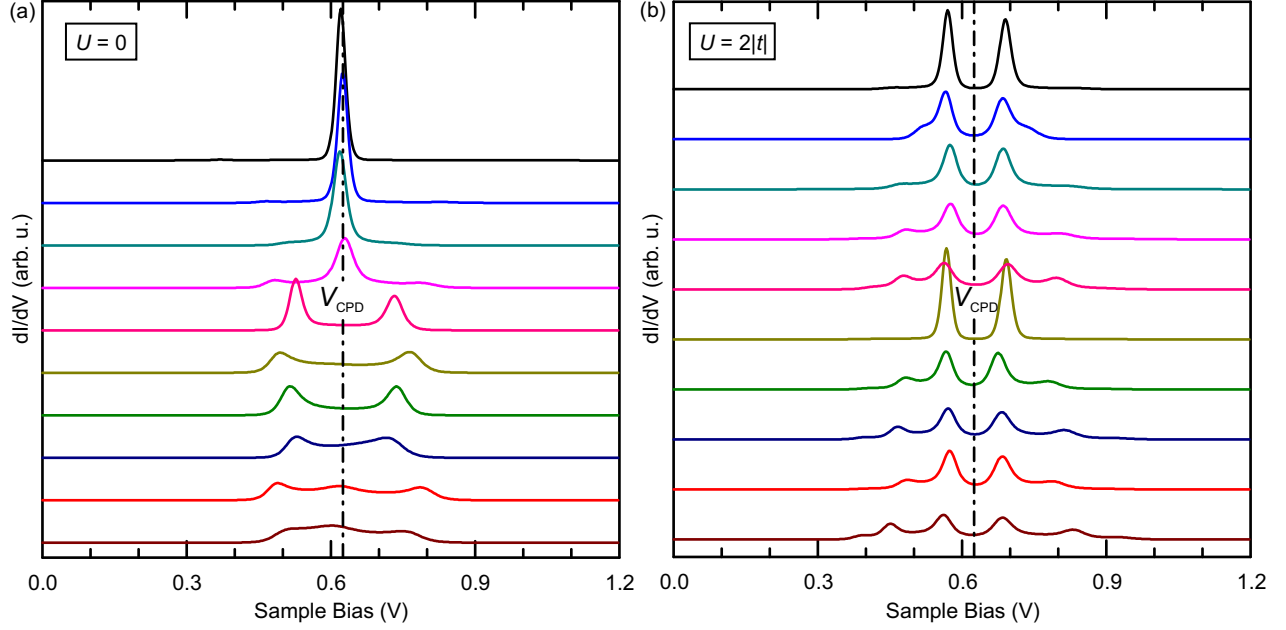


FIG. 12. Differential conductance  $dI/dV(V)$  as a function of sample bias  $V$  corresponding to different random realizations of the foremost acceptors Hamiltonian. The different traces are shifted for clarity. Both the on-site energies  $\epsilon_i$  and the inter-acceptor tunnelling parameter  $t$  are randomized. The randomization is moderate ( $\epsilon_i \pm 1$  meV) for the on-site energy and exponential (in the range 2 meV–15 meV) for the hopping parameter due to the exponential dependence of the tunnelling on the random inter-acceptor distance. In (a) the interaction is switched off while  $U = 2|t|$  in (b).

In Fig. S12 we consider instead the effect of the randomization of the on-site energy parameters  $\epsilon_i$  and tunneling amplitude  $t$  on the transport characteristics of the system. The simulation has been performed both without [Fig. S9(a)] and with Coulomb interaction [Fig. S9(b)]. In both cases the randomization produces a large variety of differential conductance traces. In the  $U = 0$  case one can distinguish 3 possible scenarios: i) a dominant peak at  $V = V_{\text{CPD}}$  associated to a weakly coupled last impurity; ii) two well separated peaks, corresponding to a bonding and anti-bonding of the two more strongly hybridized last impurities ; iii) a combination of the two previous pictures. In the finite  $U$  case the differential conductance reveals almost always 4 peaks but with strongly varying height and position.

In Fig. S13 we show last impurity population and differential conductance as a function of bias for models with (a) different number of foremost acceptors, (b) different temperatures.

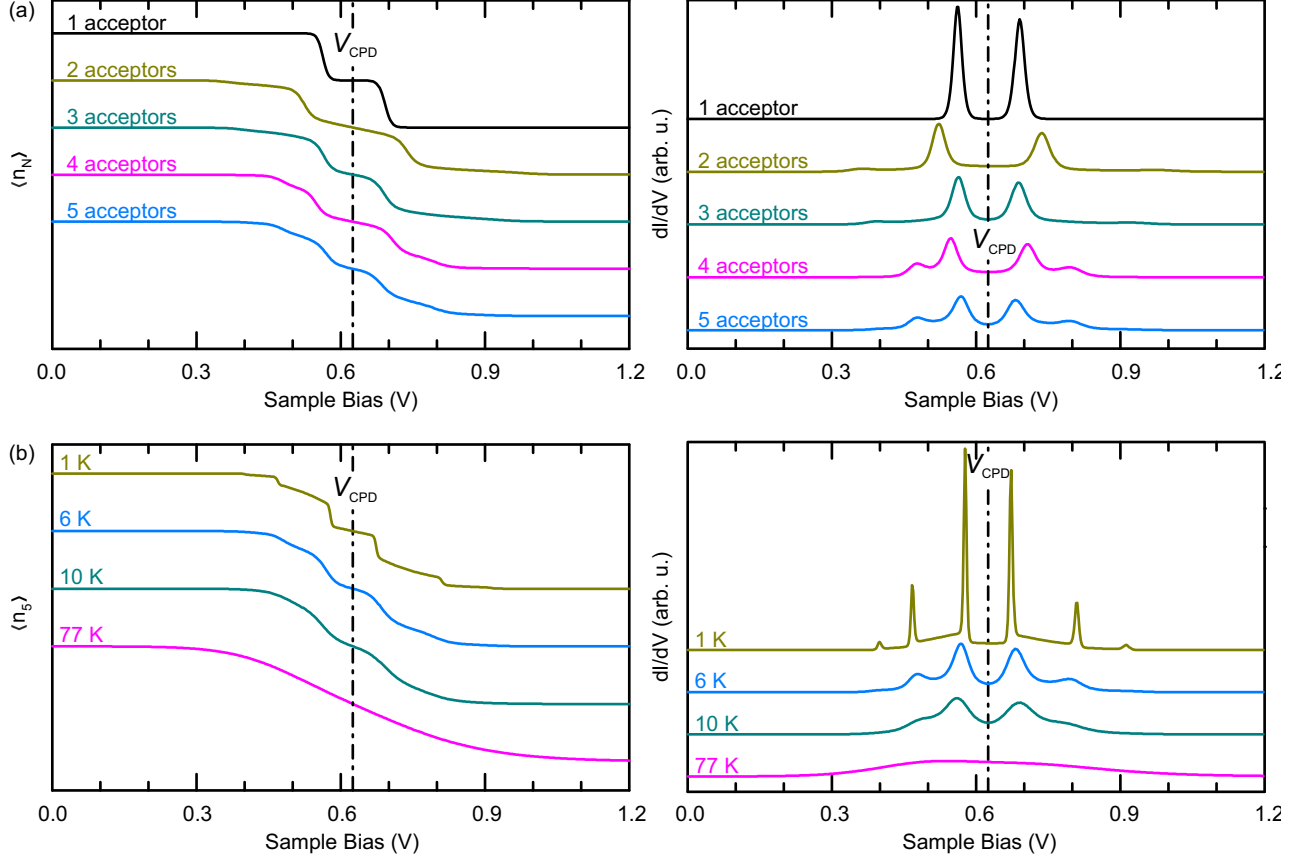


FIG. 13. (a) Last impurity population  $\langle n_N \rangle$  and differential conductance  $dI/dV(V)$  as a function of sample bias  $V$  for models with a different number of foremost acceptors  $N$ . Traces are vertically offset for clarity. (b) shows, for  $N = 5$ ,  $\langle n_5 \rangle$  and  $dI/dV(V)$  for different temperatures  $T$ . Traces are vertically offset for clarity.

The variation in the number of foremost impurities produces several effects. Firstly, when passing from the one to the two acceptor model the differential conductance peaks pass from two to four. Their number remains unchanged with increasing impurities ( $N = 3, 4, 5$ ) at least in absence of randomization. Secondly one can appreciate an even-odd effect in the distance between the two peaks closer to the flat band condition: larger distance for even acceptor numbers, smaller for odd ones. This is rationalized by observing that the single particle spectrum for an open chain of  $N$  acceptors is given by:

$$E_n = \epsilon + 2t \cos\left(\frac{\pi n}{N+1}\right) \quad (15)$$

with  $n = 1, 2, \dots, N$ . Such a spectrum has a state at the (Fermi) energy  $\epsilon$  only for odd num-

ber of impurities. In this cases the peak distance reduces to the charging energy (enlarged by the level arm factor). For even  $N$ 's one should add to the charging energy the distance of the single particle energies from the Fermi level. Thirdly, one notices a progressive closing of the gap around  $V = V_{\text{CPD}}$  while increasing the number of acceptors. This is the consequence of two facts: firstly a larger number of acceptors decreases the single particle mean level spacing; secondly, the larger number of levels  $\epsilon_i$  within the band bending window  $\text{TIBB}(V)$  increases the delocalization of the foremost impurity states even under strong band bending conditions. This fact, on the other hand, reduces the effective charging energy to pay for the changing in the population of the last impurity associated to the differential conductance peaks. The complete vanishing of this gap would only be possible with a complete delocalization of the impurity states, an absurd condition in presence of strong bend bending. This final analysis reveals the strength of the method which is intrinsically capable to capture the crossover between the delocalized flat band condition and the localized split-off configuration at no price of introducing bias dependent effective parameters.

Finally, the differential conductance illustrated in Fig. S13(b) shows the progressive smearing of the spectra with increasing temperatures. The level arm also magnify the temperature broadening and already at 77 K the conductance peaks are expected to be completely washed out.

- 
- [1] L. Gross et al., *Science* **324**, 1428 (2009).
- [2] A. J. Weymouth et al., *Phys. Rev. Lett.* **106**, 226801 (2011).
- [3] S. Sadewasser and T. Glatzel, (Eds.), *Kelvin Probe Force Microscopy* (Springer Series in Surface Science, Heidelberg, 2011), Vol. 48.
- [4] The parameters at which KPFS data were acquired on the Cu(111) surface and on the GaAs(110) surface are as follows: The tip was retracted by  $\Delta z = 5 \text{ \AA}$  after the feedback-loop of the STM was interrupted at a setpoint of  $V = 50 \text{ mV}$ ,  $I = 2.5 \text{ pA}$  [on Cu(111)], or at sample bias ranging from 1.55 V to 1.8 V at a current of  $I = 20 \text{ pA}$  [on GaAs(110)].
- [5] The standard deviations of the parabolic fits to the Kelvin parabolas are below 4 meV.
- [6] D. R. Linde (Ed.), *Handbook of Chemistry and Physics* (CRC Press, Boca Raton, 2004), 90<sup>th</sup> edition.
- [7] S. Adachi, *GaAs and Related Materials* (World Scientific Publishing, Singapore, 1999).
- [8] E. F. Schubert, *Doping in III-V Semiconductors* (Cambridge University Press, Cambridge, 1993).
- [9] S. Loth et al., *Phys. Rev. Lett.* **96**, 066403 (2006).
- [10] S. Loth et al., *Phys. Rev. B* **76**, 235318 (2007).
- [11] S. Loth, *Atomic Scale Images of Acceptors in III-V Semiconductors*, Ph.D. thesis (Universitätsverlag Göttingen, Göttingen, 2008).
- [12] A. P. Wijnheijmer et al., *J. Vac. Sci. Technol. B* **28**, 1086 (2010).
- [13] F. E. Olsson, M. Persson, J. Repp, and G. Meyer, *Phys. Rev. B* **71**, 075419 (2005).
- [14] T. König et al., *J. Phys. Chem. C* **113**, 11301 (2009).
- [15] For apex #4, the tip-sample distance was decreased by  $0.25 \text{ \AA}$  after the feedback-loop of the STM was interrupted at  $V = 1.8 \text{ V}$ ,  $I = 20 \text{ pA}$ .
- [16] Ph. Ebert et al., *Phys. Rev. Lett.* **77**, 2997 (1996).
- [17] R. de Kort et al., *Phys. Rev. B* **63**, 125336 (2001).
- [18] M. C. M. M. van der Wielen, A. J. A. van Roij, and H. van Kempen, *Phys. Rev. Lett.* **76**, 1075 (1996).
- [19] R. M. Feenstra, *J. Vac. Sci. Technol. B* **21**, 2080 (2003).
- [20] M. Berthe et al., *Phys. Rev. Lett.* **97**, 206801 (2006).

- [21] For an even number of foremost acceptors the situation would be different. In that case it costs an energy to leave the half filling even in absence of on-site Coulomb repulsion, due to the particular form of the single particle spectrum of an open linear chain. This even/odd effect is though quite irrelevant since the definition of foremost acceptors is somehow arbitrary in the flat-band condition. We choose the odd case which, due to the form of the spectrum (half-filled level at the Fermi energy) better mimics the properties of the infinite ensemble of acceptors. See also Fig. S10(a) right panel.
- [22] A. P. Wijnheijmer et al., Phys. Rev. Lett. **102**, 166101 (2009).
- [23] K. Teichmann et al., Nano Lett. **11**, 3538 (2011).